The Ultraviolet Radiation Environment of a Tropical Megacity in Transition: Mexico City 2000-2019

Adriana Ipiña,*,†,‡ Gamaliel López-Padilla,¶ Armando Retama,§ Rubén D. Piacentini,† and Sasha Madronich‖

†*Instituto de Física Rosario (CONICET-UNR), Rosario, Argentina*

‡*Centro de Ciencias de la Atmósfera, Universidad Nacional Autónoma de México, Mexico City, Mexico*

¶*Facultad de Ciencias Físico Matemáticas, Universidad Autónoma de Nuevo León, San Nicolás de los Garza, México*

§*Independent researcher, Mexico City, Mexico*

‖*National Center for Atmospheric Research, Boulder, Colorado, USA*

E-mail: ipina@ifir-conicet.gov.ar

1   **Abstract**

2   Tropical regions experience naturally high levels of UV radiation, but urban pollu-

3   tion can reduce these levels substantially. We analyzed 20 years of measurements of

4   the UV Index (UVI) at several ground-level locations in the Mexico City Metropolitan

5   Area and compared these data with UVI values derived from satellite observations of

6   ozone and clouds (but not local pollution). The ground-based measurements were sys-

7   tematically lower than the satellite-based estimates, by ca. 40% in 2000 and 25% in

8   2019. Calculations with a radiative transfer model and observed concentrations of air

pollutants explained well the difference between satellite and ground-based UVI, and showed specific contributions from aerosols, O_3, NO_2, and SO_2, in decreasing order of importance. Such large changes in UV radiation between 2000 and 2019 have important implications ranging from human health (skin cancer and cataract induction) to air pollution control (photochemical smog formation).

Introduction

Ultraviolet (UV) radiation is an important component of the urban environment, affecting human populations directly through UV exposure of skin and eyes[1–3] and less directly (but with great impact) by driving the formation of photochemical smog, including tropospheric ozone and other oxidants, as well as secondary aerosols containing nitrates, sulfates, and organics.[4–6] These pollutants, along with others of primary origin commonly found in urban atmospheres (e.g., black carbon, sulfur dioxide), can in turn scatter and/or absorb UV radiation, alter its vertical distribution, and so modify the photochemical rate of their own formation. Such feedback complicates the calculation of both the UV radiation field (including at the surface), and the evolution of photochemical smog in the urban boundary layer.

The question of how air pollution alters the urban UV radiation environment (and *vice versa*) is not new, but studies have relied mostly on numerical models,[7–9] with relatively few available observations (e.g., McKenzie et al.[10], Panicker et al.[11], Palancar et al.[12], reviewed by Bais et al.[13]). Increases in UV have been estimated as a consequence of emission reductions over the last decades, e.g. in China,[14–16] and have led to less-than-expected reductions in photochemical smog, in part due to stronger UV photochemistry.[17–19] Emission reductions have also occurred globally during the 2020 COVID-19 pandemic,[20,21] but ground-level ozone in some polluted areas has actually increased,[22,23] due at least in part to the increased UV radiation. Unfortunately, the observational data base of relevant UV radiation remains rather sparse to evaluate such model-predicted feedbacks between chemistry and

radiation.

The environment of Mexico City is of particular interest for several reasons: (1) Nearly 23 million people inhabit the Mexico City Metropolitan Area (MCMA), and the UV radiation environment has direct implications for their health, both in terms of skin/eye UV exposure and *via* photochemical smog formation. (2) As a tropical megacity, it is to some extent representative of the situation of many others, with year-round intense midday UV irradiance, a shallower atmosphere due to the city's high elevation of 2240 m above sea level, and a transition toward newer and cleaner technologies, leading to gradual improvements in air quality. (3) Air quality within MCMA has undergone extensive scrutiny, with a well-established monitoring network operating since 1986,[24] numerous intensive field campaigns to study the meteorology, emissions, and photochemistry of smog formation,[25–27] and numerical modeling incorporating the evolving knowledge.[28–31] This extensive body of knowledge provides the foundation for understanding our study.

In this work, we analyze two decades of continuous measurements of the UV Index at multiple locations within the MCMA, collected by the Secretariat of the Environment (Secretaría del Medio Ambiente, SEDEMA)[1] of the Mexico City government as part of an intensive monitoring network over the MCMA. The UV Index is defined as:

$$UVI = 40 \int_{250nm}^{400nm} E\left(\lambda, t\right) \cdot S_{er}(\lambda) d\lambda \tag{1}$$

where $E(\lambda, t)$ is the solar spectral irradiance in units of W $\cdot$m^{-2} $\cdot$nm^{-1} and $S_{er}\left(\lambda\right)$ is the erythemal sensitivity of human skin.[32,33] Multiplication by 40 was chosen historically to express the UVI in small integer numbers, but is otherwise scientifically arbitrary.

The UVI is recognized by the World Health and Meteorological Organizations (WHO and WMO) as a standardized index of UV radiation[32] for global public information. An advantage of using the UVI as (one) measure of UV radiation is that it is being increasingly observed or calculated and disseminated, enabling more objective comparisons among seasons

---

[1]https://www.sedema.cdmx.gob.mx/

⁵⁹ and locations. The UVI observations from Mexico City, considered here, are an important
⁶⁰ element of this global picture.

⁶¹   While the UVI at the surface cannot be translated directly into photolysis frequencies
⁶² for various photo-labile molecules, the spectral weighting of the UVI (ca. 300-320 nm) is
⁶³ approximately similar to that for the photolysis of ozone to singlet oxygen atoms. Other UV
⁶⁴ wavelengths are of course also important, e.g. for the photolysis of nitrogen dioxide, and
⁶⁵ may be affected differently depending on the pollutant. With these considerations and a few
⁶⁶ other caveats, UVI trends examined here can also be used to infer accompanying trends in
⁶⁷ photolysis frequencies and influences on photochemical smog formation.

Methods

Ground-based measurements

⁷⁰ The Mexico City Metropolitan Area is located at 19.4°N, 99.1°W and 2240 meters above
⁷¹ sea level (m asl), surrounded by mountain ridges exceeding 5000 m asl, with complex to-
⁷² pography and thermal inversions that inhibit winds and favor intense air pollution.[34–36] Air
⁷³ quality monitoring and surface meteorological measurements in the MCMA are conducted
⁷⁴ continuously by the Automated Atmospheric Monitoring Network (RAMA, by its Spanish
⁷⁵ acronym) of the Atmospheric Monitoring System (SIMAT, by its Spanish acronym) of the
⁷⁶ Mexico City government. Since the year 2000, UV radiometers (model 501-A, Solar Light
⁷⁷ Company Inc., Glenside, PA) detecting wavelengths between 280-400 nm have been measur-
⁷⁸ ing erythemally-weighted solar radiation. Calibration of the UV sensors has been carried out
⁷⁹ annually by comparing against a factory-calibrated reference sensor. The output voltages
⁸⁰ from the network's sensors have been compared for at least one week against the UV read-
⁸¹ ings from the reference sensor to derive new calibration factors, which typically differed from
⁸² the old ones by 2% or less. Reference sensors were also calibrated by the manufacturer and
⁸³ updated periodically (between 3 to 5 years) to reduce systematic errors due to drifts in sensi-

4

tivity. Long term calibration drifts are minimized by these yearly re-calibrations. Although

at the beginning only a few stations were in operation and varied, currently 11 stations are

recording erythemal irradiances, which are then multiplied by 40 (see Eq. 1) to give UV In-

dices. Table 1 describes the location of the stations where the UV Index has been measured.

Figure 1 shows how the radiometers of the SIMAT have been distributed over MCMA, prior-

itizing sites with higher population density. Near real-time data for each station are available

on the SIMAT official website http://www.aire.cdmx.gob.mx/default.php. Daily max-

imum values ($UVI_{\max}$) were extracted in each of the stations around solar noon from the

time interval from 11:00 h-15:00 h CST (Central Standard Time). This database with 7305

continuous days of measurements during the period 2000-2019 was analyzed.

Table 1: SIMAT stations and AERONET site*, environmental descriptors and geographical positions. Abbreviations names: Chalco (CHA), Cuautitlán (CUT), FES Acatlán (FAC), Hangares (HAN), Laboratorio de Análisis Ambiental (LAA), Merced (MER), Montecillo (MON), Milpa Alta (MPA), Pedregal (PED), San Agustín (SAG), Santa Fe (SFE), Tlalnepantla (TLA) and National Autonomous University of Mexico (UNAM*)

| Station	Environment	Lat (°N)	Lon (°W)	El (m asl)
CHO	semi-urban	19.27	98.89	2253
CUT	ecological park	19.72	99.20	2263
FAC	urban	19.48	99.24	2299
HAN	urban	19.42	99.08	2235
LAA	urban	19.48	99.15	2255
MER	downtown	19.42	99.12	2245
MON	rural	19.46	98.90	2252
MPA	rural	19.18	98.99	2594
PED	residential	19.33	99.20	2326
SAG	urban	19.53	99.03	2241
SFE	residential	19.36	99.26	2599
TLA	urban	19.53	99.20	2311
UNAM*	University city	19.33	99.18	2294
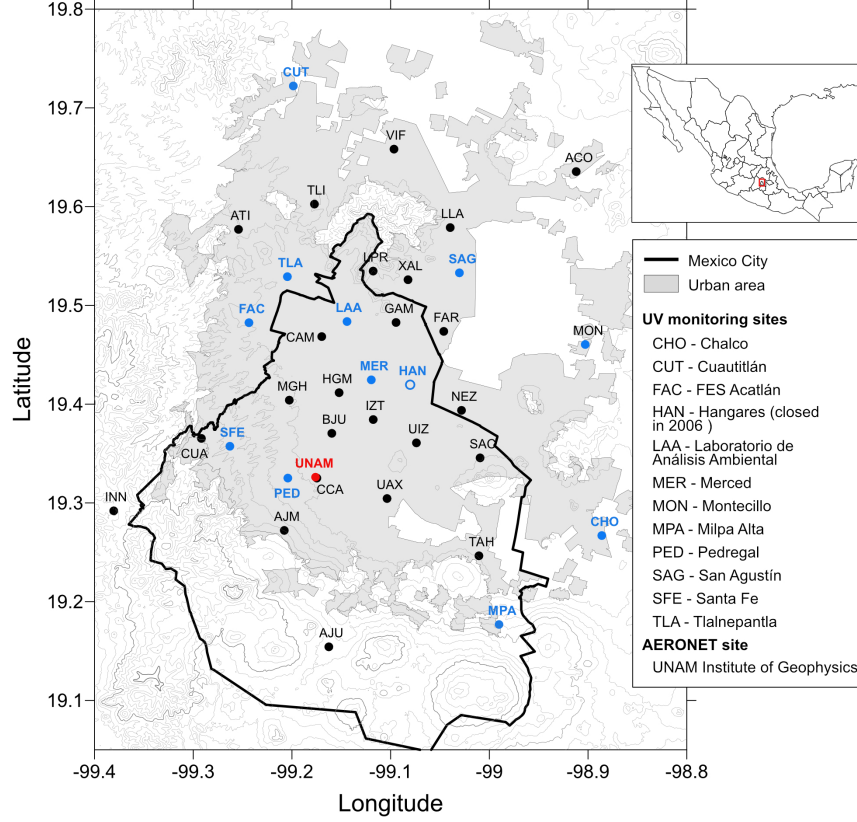
Figure 1: Map with the location of the SIMAT continuous monitoring stations over MCMA. Sites denoted by the blue solid dots correspond to SIMAT stations with UV measurements, while the black dots indicate SIMAT stations without UV measurements, the site indicated by an open blue dot represents a discontinued site, the red dot shows the location of the AERONET site. The location of Mexico City and the acronyms of the UV and AERONET site are shown at the upper and lower frames at the right respectively.

To explore the relationship between UVI and air pollutants levels, the hourly averages for ozone (O_3), carbon monoxide (CO), nitrogen dioxide (NO_2), sulfur dioxide (SO_2) and particle matter with diameter sizes ≤ 10 μm (PM_{10}), were downloaded from the SIMAT.[37] For purposes of assessing the influence on the UV Index at solar noon, only values obtained between 11h and 15h CST were considered for the trends analysis. Pollutant measurements are conducted by the SIMAT using regulatory-grade commercial instruments. Measurement principles include ultraviolet photometry (model 400E, Teledyne-API) for O_3, chemiluminescence (model 200E, Teledyne-API) for NO_2, UV fluorescence (model 100E, Teledyne API) for SO_2, and infrared absorption (model 300E, Teledyne-API) for CO. The PM_{10} continuous

6

mass concentration was measured with Tapered Element Oscillating Microbalance (TEOM 1400AB or TEOM 1405 DF, Thermo Scientific) monitors. Gaseous pollutant levels are reported in ppb concentration units for O_3, SO_2 and NO_2, and in ppm for CO. Particulate matter mass concentration is reported in μg m^{-3} at local temperature and pressure.

Aerosol optical depth at 340 nm was obtained from the Institute of Geophysics of the National Autonomous University of Mexico (UNAM). Measurements were conducted with a CIMEL sun photometer model CE-318, which is an automatic sun-sky-scanning spectral radiometer of the AErosol RObotic NETwork (AERONET[38]). The data Product Level 2.0 and 1.5 (only in 2019) were selected, and annual averages AOD_{340} were calculated for the period 2000-2019, except for the year 2011 which contained large data gaps and was therefore not used. A previous study of the AOD behavior from 2000 to 2014 demonstrated that data gaps did not significantly change the trends calculated for this time period.[39] Only 8% of the data between the years 2014 and 2019 were missing. The largest data gap occurred in 2018 when the instrument was returned for calibration.

Satellite data

The UV Index data derived from satellite-based measurements were used for comparison with the ground-based measurements. These data were provided by the Ozone Monitoring Instrument (OMI) on board of AURA-NASA satellite.[40] OMI is operated collaboratively by the Netherlands Agency for Aerospace Programmes (NIVR), the Finnish Meteorological Institute (FMI) and NASA. OMI performs observations over a geographical area of 13×24km^2 at nadir. For the coordinates (19.33°N, 99.18°W) and elevation (2268 m asl) of Mexico City, the satellite overpass time is between 19:00h - 21:00h UTC (13:00h - 15:00h CST). The OMI instrument measures reflected and backscattered radiances of the atmosphere-surface system at several UV wavelengths.[41] The ozone column is estimated by differential absorption of several adjacent wavelengths in the O_3 Huggins band[42], and is used in a radiative transfer model to estimate clear-sky UVI at the surface. Clouds are estimated from the observed

reflectivity at a wavelength not affected by O_3 absorption (360 nm) and the clear-sky UVI is adjusted for their presence.[43] A correction for absorbing aerosols is made using a global aerosol climatology.[44] The UV Index used for Mexico City corresponds to values at local noon time and clear sky from OMUVB Level 2 OVP data product, version 1.3 and collection 3.

TUV model

Calculations of the UV Index were also made with the Tropospheric Ultraviolet Visible (TUV v5.3) model.[45] The model atmosphere is represented by 80 vertical layers, each 1 km thick, starting at the 2.24 km asl elevation of MCMA, and for which the first three km constitute the atmospheric boundary layer (BL).[46] The ozone profile above the BL is from the US Standard Atmosphere, but rescaled to a value of 259.6 DU. Total ozone columns including the BL contributions (of 13.7 DU in the year 2000 and 9.8 DU in 2019, see below) were 273.1 DU in 2000 and 269.2 DU in 2019, respectively. The climatological O_3 column for this latitude and season is about 270 DU (plus or minus ca. 5 DU) so in good agreement with the values used here.

Pollutants within the BL (including O_3) are assumed to be well mixed, in agreement with observations from the MILAGRO field campaign that showed the disappearance of vertical gradients in the profiles of gases[47,48] and aerosols[49,50] by late morning. The UV-absorbing gases considered here are O_3, NO_2, and SO_2, specified in ppb.

BL aerosols are modeled by prescribing the AOD at 340 nm (from AERONET observations), scaled to other wavelengths inversely with wavelength (Angstrom coefficient = 1.0), asymmetry factor of 0.7, and a single scattering albedo of 0.85 at UV wavelengths, following the determinations made in Mexico City by Corr et al.[51] and Palancar et al.[12].

Above the atmospheric boundary layer, the model atmosphere was specified to be free of aerosols, NO_2, or SO_2. In one sensitivity study, a total AOD of 0.7 was redistributed placing 0.2 in the free troposphere (decreasing vertically with an exponential scale height of

4 km, and 0.5 remaining in the BL). The calculated UVI differed by less than 1%. Thus, as long as the total AOD is known, knowledge of the exact vertical aerosol profile is not critical for ground-level UVI, though it would obviously affect the vertical structure of photolysis frequencies.

Radiative transfer calculations were carried out with the pseudo-spherical 4-stream option, at 1 nm steps between 280 and 400 nm.

Results and Discussion

Figure 2 shows the diurnal variation of the UVI for typical cloud-free days, for different seasons and several locations (CHO, MER, MON, PED, SAG, SFE and TLA). The selection of cloud-free days was aided by comparison of the measurements with the TUV model predictions for clear skies, with prolonged deviations and fluctuations usually indicative of cloudy conditions. However, during the rainy period (from June to October) at least a brief episode of clouds is seen at CHO station around noon on 23 June 2017. Peak values range from 8 during autumn/winter to above 12 in spring/summer, in correspondence to the respective December and June solstices. Although the stations are all within a 25 km radius, substantial differences among them are notable. Survey of the locations revealed that shadowing from nearby structures is not an issue. The good agreement in the morning, followed by more divergence in the afternoon, is consistent with the development of photo-chemical pollution hotspots during the day. Previous studies (e.g., Castro et al.[52] and Palancar et al.[12]) have shown that surface UV radiation in Mexico City is attenuated significantly by aerosols. The measurements shown in Fig. 2 are consistent with this increasing pollution during the course of the day, with highest aerosol loading (and highest variability) attained in the afternoon. Further support for the role of pollution in suppressing the UVI comes from the observation made at the Santa Fe (SFE) site which in Fig. 2 are seen to be systematically higher, e.g. by over 10% in autumn afternoons, compared to the other stations. The SFE station is

9

displaced to the west from the majority of the other stations, and remains in the outskirts. This site is also approximately 300 m higher than Mexico City downtown, so that the cleaner atmosphere at SFE is a result of the station's location farther away from pollution sources, both horizontally and vertically.[53] It is indeed expected to have higher values of the UVI, in agreement with the observations.
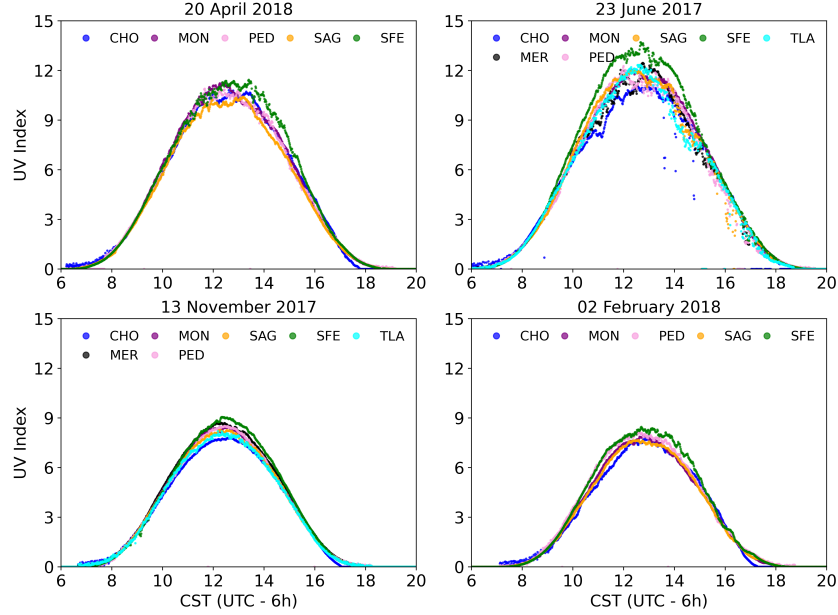

Figure 2: UV Index measurements at 1-minute resolution from several SIMAT stations within the MCMA under mostly cloudless conditions for representative days of the year.

The daily maximum UV Index values of each station, $UVI_{\max}$, are summarized in Figure 3 for the entire period 2000-2019. These values are seen to range from 1 to 16, with a majority (61%) of the days experiencing $UVI_{\max}$ values between 6 and 10, and remarkably few, less than 1%, in the 13-16 range. The lowest values are likely due to winter days with heavy cloud cover and low sun angles, and UV attenuation by pollutants could also be amplified under such conditions, due to longer photon path lengths at low sun and within clouds. The extreme sparsity of high UVI values remains surprising, and may be an indication of the rarity of extremely unpolluted days within the city.
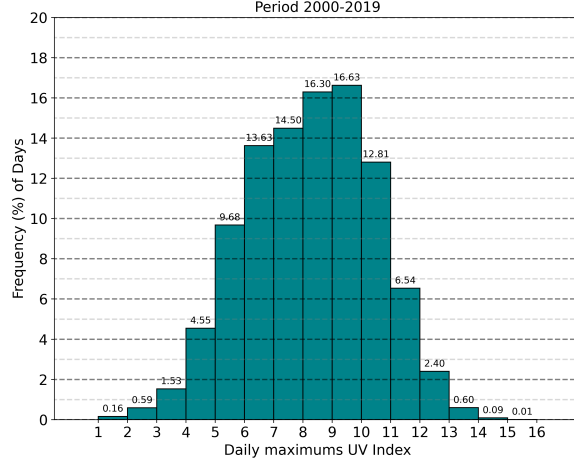
10

Figure 3: Frequency distribution of daily maximums UV Index values in Mexico City for the period 2000-2019.

Similar patterns are found when considering the monthly average of the $UVI_{\max}$ values as shown in Figure 4. The long-term averages present a seasonal variation (as in Fig. 2) that follows approximately the cosine of the noontime solar zenith angle. Notably, values rarely if ever exceed 12 (as in Fig. 3). The lowest average UVI (near 7) occurs in winter while from March to August the values seem to be flattened in the range 10-11. The rather low monthly UV Index values could be a consequence of the presence of clouds in the rainy season. However, urban aerosol pollution sources, biomass burning for agriculture and wood cooking also contribute to poor air quality between March-May[54]. Using the maximum $UVI_{\max}$ from all of stations every day (one daily point), the monthly averages ($\overline{UVI_m}$) were calculated along the period 2000-2019 (except for June 2003 due to lack of measurements). Long term trends in $\overline{UVI_m}$ are shown in Figure 5. A clear upward trend is seen, with a slope for the linear fit of 0.9%/year or +1.5 UVI units over the two decades.
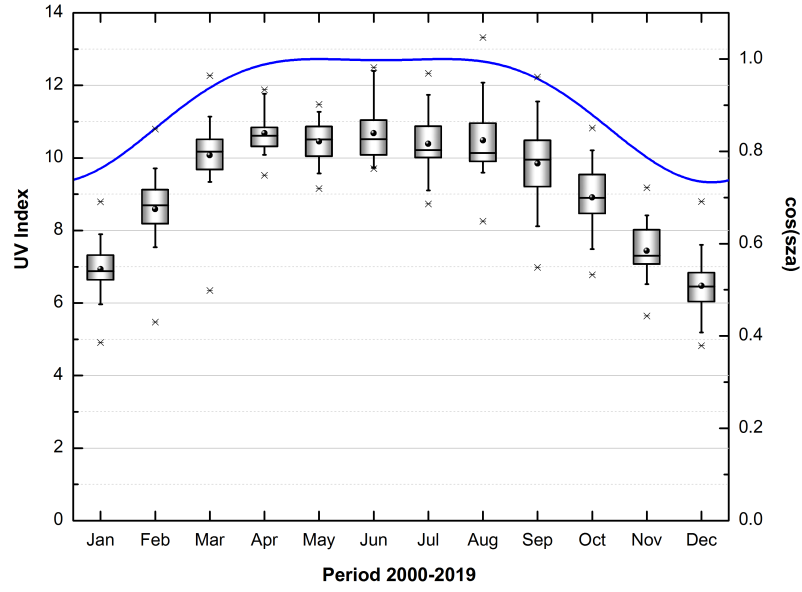
Figure 4: Monthly averages of the maximum UV Index values (black dot) in MCMA for the period 2000-2019: median (central bold line), interquartile range (box edges), 10% and 90% percentiles (whiskers), the minimum and maximum values (asterisk) and the cosine of the solar zenith angle at solar noon (blue curve).
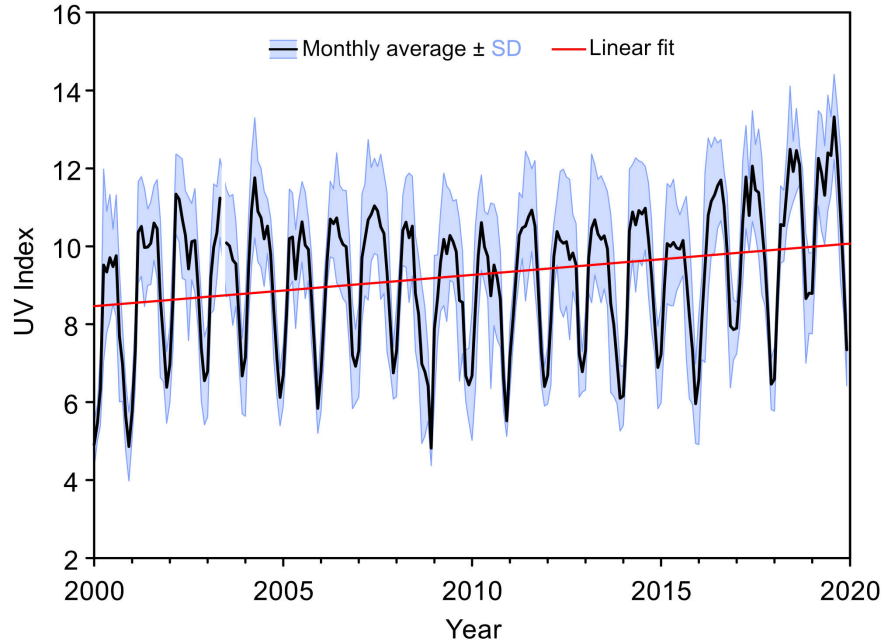
Figure 5: Monthly average UV Index (black line), the standard deviation (blue fill area) and linear fit (red line).

The UV Index computed from OMI satellite-based observations over the period 2005-2019 is shown in Figure 6. The satellite-derived UVIs vary from 8 in winter to 16 in summer, these values being substantially higher than the ground-based observations (ca. 7 for winter and 11 for summer, see Fig. 4). The maximum values are reached in June and July of each year for both data sets. We hypothesize that this large difference between satellite-based estimation and ground-based observation of the UV index is due to the intense air pollution of Mexico City. A rather similar behavior was detected in the city of Santiago, Chile.[55] Although the OMI data are corrected for climatological aerosol absorption[44], this correction likely underestimates the absorption within the polluted Mexico City BL.
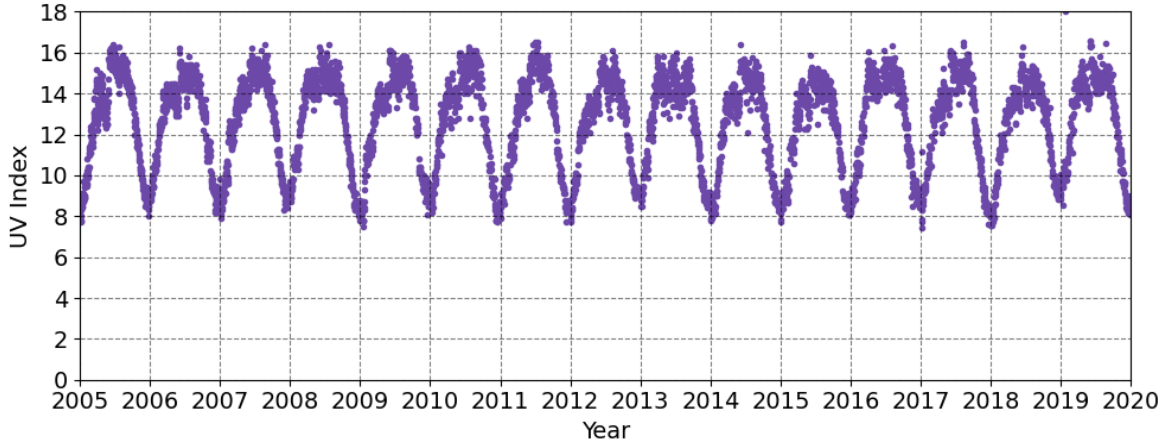
Figure 6: UV Index at solar noon for clear sky recorded by OMI-Aura/NIVR-FMI-NASA, from 2005 to 2019.
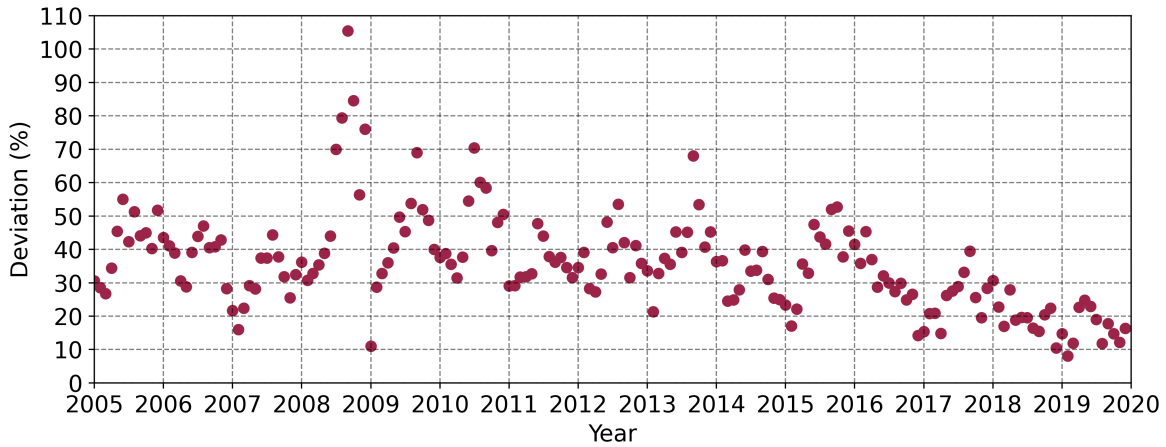

Figure 7: Deviation (%) of satellite-derived UVI from the ground-based monthly means UVI for the period 2005-2019.

Figure 7 shows the deviation of the OMI-derived UVI from the ground-based monthly averages. The mean deviation was 35% in the period 2005-2019. Comparable UV reductions, of 30-40% due to aerosols, were reported by Panicker et al.[11] over Pune, India from April 2004 to March 2005, with sensitivity coefficients (i.e. change in UVI per unit change in AOD) similar to those found here in Table 3.

Comparisons of OMI with ground-based UV measurements have been reviewed recently by Zhang et al.[56] and Vitt et al.[57]. OMI-derived UV generally overestimates ground-level

measurements by 1-10% in relatively clean conditions (e.g. rural U.S), by 10-30% in Southern Europe and by 40% or more in Santiago, Chile[55] and Thailand[58]. The overestimations appear related in large part to incomplete accounting of UV absorption by BL aerosol, although other factors such as the correction to solar noon may also introduce some bias.[56] Over Europe, ground-based UVI observations for several decades are systematically lower than those estimated from satellites even after consideration of climatological aerosol distributions, showing the importance of local pollution not resolved from space.[57] However, the difference between satellite-derived and ground-based UVI was less than 1.0 UVI units in over 90% of the cases, in contrast to the difference of 3-5 units found here for Mexico City.

Effect of pollutants on UV radiation in Mexico City

Trends and averages in aerosol optical depth AOD_{340} and criteria pollutants PM_{10}, CO, NO_2, O_3 and SO_2 observed at the SIMAT stations over 2000-2019, are shown in Figure 8 and summarized in Table 2 together with the UVI_{max}. Similar trends in pollutants have been noted before[59–61] and reflect the long-term success of emission reduction policies and programs.
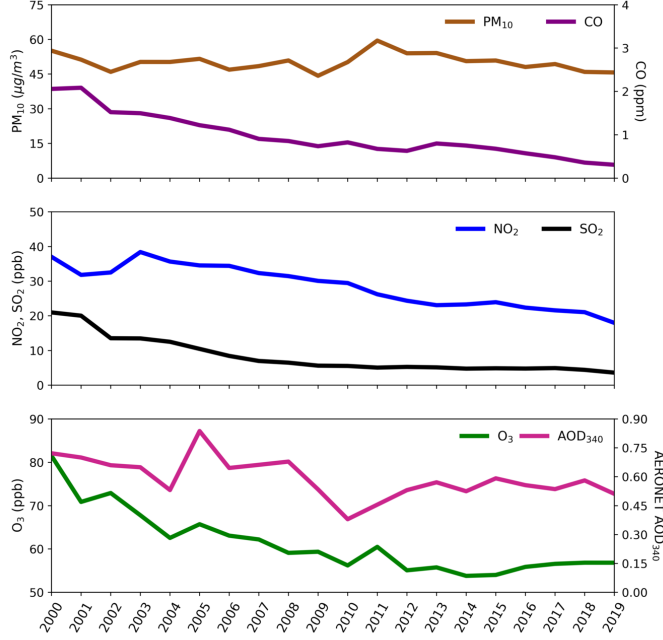
Figure 8: Air quality trends in MCMA for the period 2000-2019. Annual averages obtained between 11h to 15h CST every day: PM_{10} (brown curve), CO (purple curve), NO_2 (blue curve), SO_2(black curve), O_3 (green curve) and AOD_{340} (magenta curve).

Table 2: Trends of UV Index and criteria pollutants over 2000-2019. Units: $\mu g/m^3$ for PM_{10}, ppm for CO, ppb for SO_2, NO_2 and O_3.

Variable	$\frac{absolute\ change}{year}$	$Avg_{2000-2019}$	$\Delta(\%/year)$
UVI	0.08	9.2	0.9
PM_{10}	-0.10	50.2	-0.2
CO	-0.08	1.0	-8.2
NO_2	-0.96	28.6	-3.4
O_3	-1.05	61.3	-1.7
AOD_{340}	-0.01	0.6	-1.6
SO_2	-0.76	8.4	-9.1

²³⁶ The observed changes in the concentrations of these air pollutants have significant impli-

²³⁷ cations for surface UV radiation, as can be demonstrated with the TUV radiative transfer

²³⁸ model. Table 3 summarizes UVI values for the June-July time period, estimated by the three

²³⁹ methods: OMI satellite-derived UVI, SIMAT ground-based observations, and TUV model-

²⁴⁰ ing using air pollution estimates. Two groups of values can be readily identified: (1) SIMAT

16

daily record values, OMI with or without BL aerosols, and TUV for very clean conditions, all with UVI values around 15-16; and (2) the average of daily maxima of SIMAT observations and TUV UVI results using MCMA pollutants as input. Note that SIMAT and TUV value are in good agreement for both 2000-2001 and 2018-2019 and are considerably lower than for group (1). Compared to the OMI estimate that included the climatological absorbing aerosol correction (16.6), observed SIMAT values were lower by 40% in 2000 and by 25% in 2019. Similarly, TUV values were 35% lower in 2000 and 22% lower in 2019 relative to the TUV values of 15.6 for a pristine atmosphere.

Table 3: Comparison of June-July UVI maxima measured directly (SIMAT), inferred from satellite-based observations (OMI), and modeled for different pollution levels (TUV calculation for 21 June at solar noon).

June-July	UV Index
SIMAT average maxima 2000-2001	9.9 ± 1.2
SIMAT average maxima 2018-2019	12.3 ± 1.3
SIMAT maximum value reached in period 2000-2019	15.0
OMI maximum value reached in period 2005-2019	16.6
TUV "zero" pollution AOD 0, O_3 0 ppb, NO_2 0 ppb, SO_2 0 ppb	16.1
TUV pristine atmosphere AOD 0.05, O_3 10 ppb, NO_2 0 ppb, SO_2 0 ppb	15.6
TUV 2019: AOD 0.5, O_3 50 ppb, NO_2 20 ppb, SO_2 1 ppb	12.1
TUV 2000: AOD 0.7, O_3 70 ppb, NO_2 40 ppb, SO_2 20 ppb	10.2

The agreement between SIMAT observations and TUV model estimates is excellent but also probably a bit fortuitous. Clouds on average reduce the irradiance impingent on the surface, but scattering from them can also cause transient enhancements (these are only possible if the disk of the Sun is visible) that could be recorded as daily maxima – with cancellation between these cloud effects resulting in improved agreement with the cloud-free model. We cannot exclude that some of the observed trend in UVI is due to changes in cloud cover. However, the modeled UVI reductions due to pollutants, shown in Table 3, are in such good agreement with the observed UVI reductions, that a compelling case can be

17

₂₅₇ made for a dominant role of air pollutants in the long-term UVI trends.

₂₅₈ Table 4 shows the contribution to UVI reductions from individual pollutants, computed
₂₅₉ with the TUV model for conditions similar to those in Table 3 (21 June solar noon). If the
₂₆₀ pollutant levels of the year 2000 are added one at the time to a pollution-free atmosphere (see
₂₆₁ middle column of Table 4), aerosols account for more than half of the total UVI reduction,
₂₆₂ with the gases O_3, NO_2, and SO_2, contributing in order of importance to the remainder. It
₂₆₃ should be noted that the sum of these individual contributions (-6.8) differs from the value
₂₆₄ obtained if these pollutants are applied simultaneously rather than one at the time (-5.9, from
₂₆₅ Table 3). This non-additivity results mainly from (1) saturation of overlapping absorption
₂₆₆ spectra, especially for O_3 and SO_2 at the shortest wavelengths, and (2) interactions between
₂₆₇ absorption and scattering, e.g. aerosols causing a change in photon pathlengths through
₂₆₈ absorbing gases; both effects are treated in the TUV model.

₂₆₉ The right column of Table 4 shows the contribution of the individual pollutants to the
₂₇₀ UVI increase experienced over the years 2000-2019. For this calculation, the pollutants were
₂₇₁ decreased individually to their 2019 level while the others were held at the 2000 values.
₂₇₂ Aerosol reductions were the largest single factor responsible for the UV increase, but more
₂₇₃ than half of the increase was due to reductions of the gases, of which the near-complete
₂₇₄ elimination of SO_2 was most important. The total increase computed from the sum (1.8)
₂₇₅ is in good agreement with the 2000-2019 increase in which all pollutants were changed
₂₇₆ simultaneously (1.9, from Table 3), as smaller changes in UVI mitigate non-linearities.

Table 4: Contribution of different pollutants to UV Index changes in Mexico City, calculated
with the TUV model for 21 June at solar noon. (a) Pollutants from year 2000 added to clean
atmosphere, one at the time. (b) Pollutants lowered from 2000 to 2019 levels, one at the
time.

Pollutant	ΔUVI, 2000 - zero pollution (a)	ΔUVI, 2000-2019 (b)
AOD	-3.7	0.8
O_3	-1.4	0.3
NO_2	-0.9	0.3
SO_2	-0.8	0.4
Total	**-6.8**	**1.8**

²⁷⁷ UV reductions by air pollutants are expected to be most severe near the surface, while

²⁷⁸ chemical reactions leading to photochemical smog occur throughout the vertical extent of the

²⁷⁹ BL. Figure 9 shows the vertical profiles of photolysis coefficients (the reciprocals of photolytic

²⁸⁰ lifetimes) computed with the TUV model, for two key reactions, the photolysis of O_3 to yield

²⁸¹ excited oxygen atoms $O(^1D)$, and the photolysis of NO_2. In the absence of optically active

²⁸² pollutants, these coefficients would be nearly independent of altitude in the BL. However,

²⁸³ the presence of pollutants leads to a strong decrease toward the surface, with notably more

²⁸⁴ severe reductions in 2000 compared to 2019. While the specific values shown in the figure

²⁸⁵ are only illustrative for typical conditions, routine daily air quality modeling should carefully

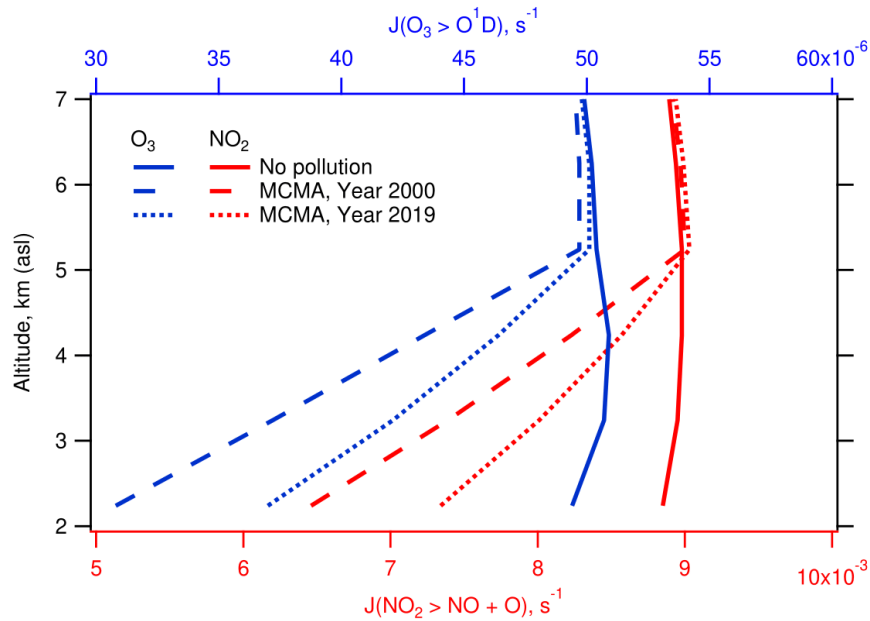²⁸⁶ account for the long term variations in these photolysis coefficients.

Figure 9: Vertical profiles of the photolysis coefficients for the reaction $O_3 + h\nu \rightarrow O(^1D) + O_2$ (top axis, blue) $NO_2 + h\nu \rightarrow O + NO$ (bottom axis, red) for zero pollution (solid) and Mexico City in the years 2000 (dashed) and 2019 (dotted). TUV calculation for 21 June at solar noon.

²⁸⁷ An issue that is beginning to gain relevance in radiative balance models is the influence

²⁸⁸ of a group of organic compounds known as "brown carbon" that are capable of strongly

²⁸⁹ absorbing in the UV region.[62] Some of these compounds are related to emissions from local

and regional wildfires.[63] Mexico City is frequently exposed to regional fire smoke transport during the dry part of the year (November to May)[64], which sporadically modify the optical properties of the aerosols.[65] This could partly explain the relatively minor reductions in PM_{10} (see Fig. 8), compared to the larger reductions of CO, NO_2, and O_3 that are more directly related to urban activities, as well as some of the seasonal asymmetry seen in Fig. 3.

The UVI is specific to wavelengths mainly in the 300-320 nm range, and so the question remains whether these results can be applied at longer UV wavelengths, e.g. those important for NO_2 photolysis (<420 nm). Absorption by SO_2 and O_3 vanishes for wavelengths larger than about 330 nm, while NO_2 photolysis is mostly driven by UV-A radiation and typical aerosols optical depth decrease with wavelength. These changes can easily be modeled, but unfortunately far fewer measurements of these longer wavelengths are available in Mexico City or elsewhere.

Two decades of observations in Mexico City demonstrate unequivocally that air pollution reduces UV radiation at the ground. The ground-based observations are well below values derived from satellite-based observations. Although ideally both data sets should match, the limited ability of satellites to detect BL absorbers means that they cannot reveal long-term UV trends. Thus, they do not reveal long-term UVI trends, due to substantial air quality improvemnets, that are evident in the ground-based UVI data. When typical values of pollutant aerosols, tropospheric ozone, NO_2 and SO_2, are included in a model (e.g. TUV), the differences between satellite-derived and ground-based measured values are explained and can be attributed quantitatively to individual observed pollutants. Long term improvements in air quality over the last two decades were accompanied by statistically significant increases in the observed UVI, in agreement with the model-predicted changes.

The reductions in surface UV radiation with respect to an ideally clear atmosphere – by nearly 40% in 2000 and still 20% in 2019 – are large, both within the context of human UV exposure and air quality mitigation. In urban areas where ozone production scales

proportionally with UV levels and with volatile organic compound (VOC) emissions (the VOC-limited regime), a 10% increase in BL average photolysis rates means that VOC emissions will need to be reduced by 10% to meet the same goals, or else successful reductions in aerosols would lead to unwanted UV-driven increases in O_3. Such UV changes must be considered carefully in air quality mitigation strategies. For human exposure, a 20% increase in UV irradiances over two decades should be seen as a non-negligible public health issue requiring some reassessment of preventive behaviors to minimize the risk of skin cancer, cataract, and other UV-related health effects. The efforts that Mexico City has made to improve air quality have reduced levels of most air pollutants. Nevertheless, they caused an increase in UV radiation that reaches the surface.

Finally, based on our results, the solar radiation monitoring network might be improved by adding observation sites far enough away to lessen the influence of the urban plume (e. g., Amecameca; latitude: 19.13°N, longitude: 99.76°W, elevation: 2420 m asl), and the adding sensors to existing monitoring sites at higher elevations (Ajusco, AJU, 2953 m asl or Instituto de Investigaciones Nucleares, INN, 3082 m asl). These sites would provide valuable observations to assess quantitatively the effects of urban pollution on solar radiation levels.

Acknowledgement

References

(1) Taylor, H. R.; West, S. K.; Rosenthal, F. S.; Muñoz, B.; Newland, H. S.; Abbey, H.; Emmett, E. A. Effect of Ultraviolet Radiation on Cataract Formation. *New England Journal of Medicine* **1988**, *319*, 1429–1433.

(2) Varotsos, C.; Feretis, E. Health effects on human eye resulting from the increased ambient solar ultraviolet radiation. *Toxicological & Environmental Chemistry* **1997**, *61*, 43–68.

(3) Lucas, R. M.; Yazar, S.; Young, A. R.; Norval, M.; de Gruijl, F. R.; Takizawa, Y.; Rhodes, L. E.; Sinclair, C. A.; Neale, R. E. Human health in relation to exposure to solar ultraviolet radiation under changing stratospheric ozone and climate. *Photochemical & Photobiological Sciences* **2019**, *18*, 641–680.

(4) Leighton, P. A. *Photochemistry of Air Pollution*; Elsevier, 1961; pp v–vi.

(5) Seinfeld, J. H.; Pandis, S. N.; Noone, K. Atmospheric Chemistry and Physics: From Air Pollution to Climate Change. *Physics Today* **1998**, *51*, 88–90.

(6) Finlayson-Pitts, B. J.; Pitts, J. N. *Chemistry of the Upper and Lower Atmosphere*; Academic Press, 2000; pp xvii–xviii.

(7) Liu, S. C.; McKeen, S. A.; Madronich, S. Effect of anthropogenic aerosols on biologically active ultraviolet radiation. *Geophysical Research Letters* **1991**, *18*, 2265–2268.

(8) Sabziparvar, A. A.; Forster, P. M. F.; Shine, K. P. Changes in ultraviolet radiation due to stratospheric and tropospheric ozone changes since preindustrial times. *Journal of Geophysical Research: Atmospheres* **1998**, *103*, 26107–26113.

(9) Madronich, S.; Wagner, M.; Groth, P. Influence of Tropospheric Ozone Control on Exposure to Ultraviolet Radiation at the Surface. *Environmental Science & Technology* **2011**, *45*, 6919–6923.

(10) McKenzie, R. L.; Weinreis, C.; Johnston, P. V.; Liley, B.; Shiona, H.; Kotkamp, M.; Smale, D.; Takegawa, N.; Kondo, Y. Effects of urban pollution on UV spectral irradiances. *Atmospheric Chemistry and Physics* **2008**, *8*, 5683–5697.

(11) Panicker, A. S.; Pandithurai, G.; Takamura, T.; Pinker, R. T. Aerosol effects in the UV-B spectral region over Pune an urban site in India. *Geophysical Research Letters* **2009**, *36*, L10802 1–5.

(12) Palancar, G. G.; Lefer, B. L.; Hall, S. R.; Shaw, W. J.; Corr, C. A.; Herndon, S. C.; Slusser, J. R.; Madronich, S. Effect of aerosols and NO_2 concentration on ultraviolet actinic flux near Mexico City during MILAGRO: measurements and model calculations. *Atmospheric Chemistry and Physics* **2013**, *13*, 1011–1022.

(13) Bais, A. F.; McKenzie, R. L.; Bernhard, G.; Aucamp, P. J.; Ilyas, M.; Madronich, S.; Tourpali, K. Ozone depletion and climate change: impacts on UV radiation. *Photochemical & Photobiological Sciences* **2015**, *14*, 19–52.

(14) Hollaway, M.; Wild, O.; Yang, T.; Sun, Y.; Xu, W.; Xie, C.; Whalley, L.; Slater, E.; Heard, D.; Liu, D. Photochemical impacts of haze pollution in an urban environment. *Atmospheric Chemistry and Physics* **2019**, *19*, 9699–9714.

(15) Li, K.; Jacob, D. J.; Liao, H.; Shen, L.; Zhang, Q.; Bates, K. H. Anthropogenic drivers of 2013–2017 trends in summer surface ozone in China. *Proceedings of the National Academy of Sciences* **2018**, *116*, 422–427.

(16) Wang, Y.; Gao, W.; Wang, S.; Song, T.; Gong, Z.; Ji, D.; Wang, L.; Liu, Z.; Tang, G.; Huo, Y.; Tian, S.; Li, J.; Li, M.; Yang, Y.; Chu, B.; Petäjä, T.; Kerminen, V.-M.; He, H.; Hao, J.; Kulmala, M.; Wang, Y.; Zhang, Y. *Contrasting trends of PM2.5 and surface-ozone concentrations in China from 2013 to 2017*; Oxford University Press (OUP), 2020; Vol. 7; pp 1331–1339.

(17) Wang, W.; Li, X.; Shao, M.; Hu, M.; Zeng, L.; Wu, Y.; Tan, T. The impact of aerosols on photolysis frequencies and ozone production in Beijing during the 4-year period 2012–2015. *Atmospheric Chemistry and Physics* **2019**, *19*, 9413–9429.

(18) Gao, J.; Li, Y.; Zhu, B.; Hu, B.; Wang, L.; Bao, F. What have we missed when studying the impact of aerosols on surface ozone via changing photolysis rates? *Atmospheric Chemistry and Physics* **2020**, *20*, 10831–10844.

(19) Ma, X.; Huang, J.; Zhao, T.; Liu, C.; Zhao, K.; Xing, J.; Xiao, W. Rapid increase in summer surface ozone over the North China Plain during 2013–2019: a side effect of particulate matters reduction control? *Atmospheric Chemistry and Physics* **2021**, *21*, 1–16.

(20) Bauwens, M.; Compernolle, S.; Stavrakou, T.; Müller, J.-F.; Gent, J.; Eskes, H.; Levelt, P. F.; A, R.; Veefkind, J. P.; Vlietinck, J.; Yu, H.; Zehner, C. Impact of coronavirus outbreak on NO2 pollution assessed using TROPOMI and OMI observations. **2020**, *47*, e2020GL087978.

(21) Venter, Z. S.; Aunan, K.; Chowdhury, S.; Lelieveld, J. COVID-19 lockdowns cause global air pollution declines. *Proceedings of the National Academy of Sciences* **2020**, *117*, 18984–18990.

(22) Shi, X.; Brasseur, G. P. The Response in Air Quality to the Reduction of Chinese Economic Activities During the COVID-19 Outbreak. *Geophysical Research Letters* **2020**, *47*, e2020GL088070.

(23) Le, T.; Wang, Y.; Liu, L.; Yang, J.; Yung, Y. L.; Li, G.; Seinfeld, J. H. Unexpected air pollution with marked emission reductions during the COVID-19 outbreak in China. *Science* **2020**, *369*, 702–706.

(24) Secretaría del Medio Ambiente, Gobierno de la Ciudad de México, México, Red

Automática de Monitoreo Atmosférico (RAMA). http://www.aire.cdmx.gob.mx/descargas/datos/excel/RAMAxls.pdf.

(25) Doran, J. C.; Abbott, S.; Archuleta, J.; Bian, X.; Chow, J.; Coulter, R. L.; de Wekker, S. F. J.; Edgerton, S.; Elliott, S.; Fernandez, A.; Fast, J. D.; Hubbe, J. M.; King, C.; Langley, D.; Leach, J.; Lee, J. T.; Martin, T. J.; Martinez, D.; Martinez, J. L.; Mercado, G.; Mora, V.; Mulhearn, M.; Pena, J. L.; Petty, R.; Porch, W.; Russell, C.; Salas, R.; Shannon, J. D.; Shaw, W. J.; Sosa, G.; Tellier, L.; Templeman, B.; Watson, J. G.; White, R.; Whiteman, C. D.; Wolfe, D. The IMADA-AVER Boundary Layer Experiment in the Mexico City Area. *Bulletin of the American Meteorological Society* **1998**, *79*, 2497–2508.

(26) Molina, L. T.; Kolb, C. E.; de Foy, B.; Lamb, B. K.; Brune, W. H.; Jimenez, J. L.; Ramos-Villegas, R.; Sarmiento, J.; Paramo-Figueroa, V. H.; Cardenas, B.; Gutierrez-Avedoy, V.; Molina, M. J. Air quality in North America's most populous city – overview of the MCMA-2003 campaign. *Atmospheric Chemistry and Physics* **2007**, *7*, 2447–2473.

(27) Molina, L. T.; Madronich, S.; Gaffney, J. S.; Apel, E.; de Foy, B.; Fast, J.; Ferrare, R.; Herndon, S.; Jimenez, J. L.; Lamb, B.; Osornio-Vargas, A. R.; Russell, P.; Schauer, J. J.; Stevens, P. S.; Volkamer, R.; Zavala, M. An overview of the MILAGRO 2006 Campaign: Mexico City emissions and their transport and transformation. *Atmospheric Chemistry and Physics* **2010**, *10*, 8697–8760.

(28) Jazcilevich, A. D.; García, A. R.; Caetano, E. Locally induced surface air confluence by complex terrain and its effects on air pollution in the valley of Mexico. *Atmospheric Environment* **2005**, *39*, 5481–5489.

(29) Tie, X.; Madronich, S.; Li, G.; Ying, Z.; Zhang, R.; Garcia, A. R.; Lee-Taylor, J.; Liu, Y. Characterizations of chemical oxidants in Mexico City: A regional chemical dynamical model (WRF-Chem) study. *Atmospheric Environment* **2007**, *41*, 1989–2008.

(30) Zhang, Y.; Dubey, M. K.; Olsen, S. C.; Zheng, J.; Zhang, R. Comparisons of WRF/Chem simulations in Mexico City with ground-based RAMA measurements during the 2006-MILAGRO. *Atmospheric Chemistry and Physics* **2009**, *9*, 3777–3798.

(31) Zavala, M.; Brune, W. H.; Velasco, E.; Retama, A.; Cruz-Alavez, L. A.; Molina, L. T. Changes in ozone production and VOC reactivity in the atmosphere of the Mexico City Metropolitan Area. *Atmospheric Environment* **2020**, *238*, 117747.

(32) WHO,; WMO,; UNEP,; ICNIRP, *Global solar UV index : a practical guide*; 2002; pp A joint recommendation of the World Health Organization, World Meteorological Organization, United Nations Environment Programme, and the International Commission on Non–Ionizing Radiation Protection.

(33) Webb, A. R.; Slaper, H.; Koepke, P.; Schmalwieser, A. W. Know Your Standard: Clarifying the CIE Erythema Action Spectrum. *Photochemistry and Photobiology* **2011**, *87*, 483–486.

(34) Whiteman, C. D.; Zhong, S.; Bian, X.; Fast, J. D.; Doran, J. C. Boundary layer evolution and regional-scale diurnal circulations over the and Mexican plateau. *Journal of Geophysical Research: Atmospheres* **2000**, *105*, 10081–10102.

(35) Fast, J. D.; de Foy, B.; Rosas, F. A.; Caetano, E.; Carmichael, G.; Emmons, L.; McKenna, D.; Mena, M.; Skamarock, W.; Tie, X.; Coulter, R. L.; Barnard, J. C.; Wiedinmyer, C.; Madronich, S. A meteorological overview of the MILAGRO field campaigns. *Atmospheric Chemistry and Physics* **2007**, *7*, 2233–2257.

(36) Carreón-Sierra, S.; Salcido, A.; Castro, T.; Celada-Murillo, A.-T. Cluster Analysis of the Wind Events and Seasonal Wind Circulation Patterns in the Mexico City Region. *Atmosphere* **2015**, *6*, 1006–1031.

(37) Sistema de Monitoreo Atmosférico,Ciudad de México. http://www.aire.cdmx.gob.

463 `mx/default.php?opc=%27aKBhnmI%27&opcion=Zg`, Accessed on Wed, December 02,
464 2020.

465 (38) Holben, B.; Eck, T.; Slutsker, I.; Tanré, D.; Buis, J.; Setzer, A.; Vermote, E.; Reagan, J.;
466 Kaufman, Y.; Nakajima, T.; Lavenu, F.; Jankowiak, I.; Smirnov, A. AERONET—A
467 Federated Instrument Network and Data Archive for Aerosol Characterization. *Remote*
468 *Sensing of Environment* **1998**, *66*, 1–16.

469 (39) Carabali, G.; Estévez, H. R.; Valdés-Barrón, M.; Bonifaz-Alfonzo, R.; Riveros-
470 Rosas, D.; Velasco-Herrera, V. M.; Vázquez-Gálvez, F. A. Aerosol climatology over
471 the Mexico City basin: Characterization of optical properties. *Atmospheric Research*
472 **2017**, *194*, 190–201.

473 (40) NASA EOS/Aura Validation Data Center (AVDC) - Correlative data, Field of
474 View Predictions, Data Subsets, GEOMS, DCIO. `https://avdc.gsfc.nasa.gov/pub/`
475 `most_popular/overpass/OMI/`.

476 (41) Tanskanen, A.; Krotkov, N.; Herman, J.; Arola, A. Surface ultraviolet irradiance from
477 OMI. *IEEE Transactions on Geoscience and Remote Sensing* **2006**, *44*, 1267–1271.

478 (42) Veefkind, J. P.; de Haan, J. F.; Brinksma, E. J.; Kroon, M.; Levelt, P. F. Total Ozone
479 From the Ozone Monitoring Instrument (OMI) Using the DOAS Technique. *IEEE*
480 *Transactions on Geoscience and Remote Sensing* **2006**, *44*, 1239–1244.

481 (43) Tanskanen, A.; Lindfors, A.; Määttä, A.; Krotkov, N.; Herman, J.; Kaurola, J.;
482 Koskela, T.; Lakkala, K.; Fioletov, V.; Bernhard, G.; McKenzie, R.; Kondo, Y.;
483 O'Neill, M.; Slaper, H.; den Outer, P.; Bais, A. F.; Tamminen, J. Validation of daily ery-
484 themal doses from Ozone Monitoring Instrument with ground-based UV measurement
485 data. *Journal of Geophysical Research: Atmospheres* **2007**, *112*, D24S44 1–15.

486 (44) Arola, A.; Kazadzis, S.; Lindfors, A.; Krotkov, N.; Kujanpää, J.; Tamminen, J.;
487 Bais, A.; di Sarra, A.; Villaplana, J. M.; Brogniez, C.; Siani, A. M.; Janouch, M.;

Weihs, P.; Webb, A.; Koskela, T.; Kouremeti, N.; Meloni, D.; Buchard, V.; Auriol, F.; Ialongo, I.; Staneck, M.; Simic, S.; Smedley, A.; Kinne, S. A new approach to correct for absorbing aerosols in OMI UV. *Geophysical Research Letters* **2009**, *36*, L22805 1–5.

(45) Madronich, S. Intercomparison of NO2 photodissociation and U.V. Radiometer Measurements. *Atmospheric Environment* **1987**, *21*, 569–578.

(46) Shaw, W. J.; Pekour, M. S.; Coulter, R. L.; Martin, T. J.; Walters, J. T. The daytime mixing layer observed by radiosonde profiler, and lidar during MILAGRO. *Atmospheric Chemistry and Physics Discussions* **2007**, *7*, 15025–15065.

(47) Velasco, E.; Márquez, C.; Bueno, E.; Bernabé, R. M.; Sánchez, A.; Fentanes, O.; Wöhrnschimmel, H.; Cárdenas, B.; Kamilla, A.; Wakamatsu, S.; Molina, L. T. Vertical distribution of ozone and VOCs in the low boundary layer of Mexico City. *Atmospheric Chemistry and Physics* **2008**, *8*, 3061–3079.

(48) Greenberg, J.; Guenther, A.; Turnipseed, A. Tethered balloon-based soundings of ozone aerosols, and solar radiation near Mexico City during MIRAGE-MEX. *Atmospheric Environment* **2009**, *43*, 2672–2677.

(49) Rogers, R. R.; Hair, J. W.; Hostetler, C. A.; Ferrare, R. A.; Obland, M. D.; Cook, A. L.; Harper, D. B.; Burton, S. P.; Shinozuka, Y.; McNaughton, C. S.; Clarke, A. D.; Redemann, J.; Russell, P. B.; Livingston, J. M.; Kleinman, L. I. NASA LaRC airborne high spectral resolution lidar aerosol measurements during MILAGRO: observations and validation. *Atmospheric Chemistry and Physics* **2009**, *9*, 4811–4826.

(50) Lewandowski, P. A.; Eichinger, W. E.; Holder, H.; Prueger, J.; Wang, J.; Kleinman, L. I. Vertical distribution of aerosols in the vicinity of Mexico City during MILAGRO-2006 Campaign. *Atmospheric Chemistry and Physics* **2010**, *10*, 1017–1030.

(51) Corr, C. A.; Krotkov, N.; Madronich, S.; Slusser, J. R.; Holben, B.; Gao, W.; Flynn, J.; Lefer, B.; Kreidenweis, S. M. Retrieval of aerosol single scattering albedo at ultraviolet

wavelengths at the T1 site during MILAGRO. *Atmospheric Chemistry and Physics* **2009**, *9*, 5813–5827.

(52) Castro, T.; Madronich, S.; Rivale, S.; Muhlia, A.; Mar, B. The influence of aerosols on photochemical smog in Mexico City. *Atmospheric Environment* **2001**, *35*, 1765–1772.

(53) SEDEMA, *Calidad del aire en la Ciudad de México, Informe 2017*; 2018.

(54) Retama, A.; Baumgardner, D.; Raga, G. B.; McMeeking, G. R.; Walker, J. W. Seasonal and diurnal trends in black carbon properties and co-pollutants in Mexico City. *Atmospheric Chemistry and Physics* **2015**, *15*, 9693–9709.

(55) Cabrera, S.; Ipiña, A.; Damiani, A.; Cordero, R. R.; Piacentini, R. D. UV index values and trends in Santiago Chile (33.5°S) based on ground and satellite data. *Journal of Photochemistry and Photobiology B: Biology* **2012**, *115*, 73–84.

(56) Zhang, H.; Wang, J.; García, L. C.; Zeng, J.; Dennhardt, C.; Liu, Y.; Krotkov, N. A. Surface erythemal UV irradiance in the continental United States derived from ground-based and OMI observations: quality assessment trend analysis and sampling issues. *Atmospheric Chemistry and Physics* **2019**, *19*, 2165–2181.

(57) Vitt, R.; Laschewski, G.; Bais, A.; Diémoz, H.; Fountoulakis, I.; Siani, A.-M.; Matzarakis, A. UV-Index Climatology for Europe Based on Satellite Data. *Atmosphere* **2020**, *11*, 727.

(58) Janjai, S.; Wisitsirikun, S.; Buntoung, S.; Pattarapanitchai, S.; Wattan, R.; Masiri, I.; Bhattarai, B. K. Comparison of UV index from Ozone Monitoring Instrument (OMI) with multi-channel filter radiometers at four sites in the tropics: effects of aerosols and clouds. *International Journal of Climatology* **2013**, *34*, 453–461.

(59) Parrish, D. D.; Singh, H. B.; Molina, L.; Madronich, S. Air quality progress in North American megacities: A review. *Atmospheric Environment* **2011**, *45*, 7015–7025.

(60) Secretaría del Medio Ambiente de la Ciudad de México, *Calidad del aire en la Ciudad de México, informe 2017*; 2018; pp 1–160.

(61) Molina,; Velasco,; Retama,; Zavala, Experience from Integrated Air Quality Management in the Mexico City Metropolitan Area and Singapore. *Atmosphere* **2019**, *10*, 512.

(62) Laskin, A.; Laskin, J.; Nizkorodov, S. A. Chemistry of Atmospheric Brown Carbon. *Chemical Reviews* **2015**, *115*, 4335–4382.

(63) Gadhavi, H.; Jayaraman, A. Absorbing aerosols: contribution of biomass burning and implications for radiative forcing. *Annales Geophysicae* **2010**, *28*, 103–111.

(64) Rios, B.; Raga, G. B. Smoke emissions from agricultural fires in Mexico and Central America. *Journal of Applied Remote Sensing* **2019**, *13*, 1.

(65) Barnard, J. C.; Volkamer, R.; Kassianov, E. I. Estimation of the mass absorption cross section of the organic carbon component of aerosols in the Mexico City Metropolitan Area. *Atmospheric Chemistry and Physics* **2008**, *8*, 6665–6679.

Graphical TOC Entry

Some journals require a graphical entry for the Table of Contents. This should be laid out "print ready" so that the sizing of the text is correct.

Inside the `tocentry` environment, the font used is Helvetica 8 pt, as required by *Journal of the American Chemical Society*.

The surrounding frame is 9 cm by 3.5 cm, which is the maximum permitted for *Journal of the American Chemical Society* graphical table of content entries. The box will not resize if the content is too big: instead it will overflow the edge of the box.

This box and the associated title will always be printed on a separate page at the end of the document.